JEM Journal of Experimental Medicine

BRIEF DEFINITIVE REPORT

Transcription factor Etv6 regulates functional differentiation of cross-presenting classical dendritic cells

Colleen M. Lau[1*], Ioanna Tiniakou[1*], Oriana A. Perez[1], Margaret E. Kirkling[1,2], George S. Yap[3], Hanno Hock[4], and Boris Reizis[1]

An IRF8-dependent subset of conventional dendritic cells (cDCs), termed cDC1, effectively cross-primes CD8⁺ T cells and facilitates tumor-specific T cell responses. Etv6 is an ETS family transcription factor that controls hematopoietic stem and progenitor cell (HSPC) function and thrombopoiesis. We report that like HSPCs, cDCs express Etv6, but not its antagonist, ETS1, whereas interferon-producing plasmacytoid dendritic cells (pDCs) express both factors. Deletion of Etv6 in the bone marrow impaired the generation of cDC1-like cells in vitro and abolished the expression of signature marker CD8α on cDC1 in vivo. Moreover, Etv6-deficient primary cDC1 showed a partial reduction of cDC-specific and cDC1-specific gene expression and chromatin signatures and an aberrant up-regulation of pDC-specific signatures. Accordingly, DC-specific Etv6 deletion impaired CD8⁺ T cell cross-priming and the generation of tumor antigen–specific CD8⁺ T cells. Thus, Etv6 optimizes the resolution of cDC1 and pDC expression programs and the functional fitness of cDC1, thereby facilitating T cell cross-priming and tumor-specific responses.

Introduction

Dendritic cells (DCs) link innate and adaptive immunity by recognizing pathogens through pattern recognition receptors such as TLRs and orchestrating antigen-specific T cell responses (Steinman, 2012). DCs in the steady-state lymphoid tissues are represented by two main types: IFN-producing plasmacytoid DCs (pDCs) and antigen-presenting classical or conventional DCs (cDCs). In the mouse, cDCs are composed of two main subsets: CD8α⁺/CD103⁺ cDCs capable of antigen cross-presentation to CD8⁺ T cells and CD11b⁺ "myeloid" cDCs specialized in the presentation of exogenous antigen to CD4⁺ T cells (Merad et al., 2013; Mildner and Jung, 2014; Schraml and Reis e Sousa, 2015). To reflect the genetic and functional conservation of the two cDC subsets in animals and humans, cross-presenting DCs have been recently designated as cDC1 and myeloid DCs as cDC2 (Guilliams et al., 2014). The cross-priming function of cDC1 appears particularly important for the initiation of productive antitumor CD8⁺ T cell responses (Hildner et al., 2008; Fuertes et al., 2011; Roberts et al., 2016; Salmon et al., 2016; Spranger et al., 2017).

DC development is driven by the cytokine FLT3 ligand (FLT3L) and its receptor, FLT3, as well as by a network of transcription factors that specify the differentiation of DC subsets. The development of cDC1 is strictly dependent on IRF8 (Aliberti et al., 2003; Sichien et al., 2016) and is facilitated by additional transcription factors, including BATF3 (Hildner et al., 2008) and ID2 (Hacker et al., 2003). Terminal differentiation of splenic cDC1, including the expression of CD8α, is facilitated by NOTCH2 receptor signaling (Lewis et al., 2011; Satpathy et al., 2013; Kirkling et al., 2018). The development of pDCs is similarly controlled by IRF8, which is required for their FLT3L-driven development in vitro (Aliberti et al., 2003) and IFN-producing capacity in vivo (Sichien et al., 2016). Notably, cDC1 and pDCs share several common features, including developmental and/or functional dependence on IRF8, prominent cytokine production capacity (IL-12 in cDC1 and IFN-α in pDCs), and certain functional receptors (e.g., Clec9A and Cxcr3). However, the mechanisms that resolve the unique lineage identities of the two subsets remain poorly understood. Furthermore, little is known about the factors that control terminal differentiation of cDC1, including their unique cross-presentation capacity. Such yet-unidentified factors would be expected to indirectly facilitate CD8+ T cell cross-priming to cell-associated antigens, thereby promoting tumor-specific T cell responses in cancer.

[1]Department of Pathology, New York University School of Medicine, New York, NY; [2]Graduate Program in Genetics and Development, Columbia University Medical Center, New York, NY; [3]Department of Medicine, Rutgers New Jersey Medical School, Newark, NJ; [4]Massachusetts General Hospital, Harvard Medical School, Boston, MA.

*C.M. Lau and I. Tiniakou contributed equally to this paper; Correspondence to Boris Reizis: boris.reizis@nyumc.org; C.M. Lau's present address is Immunology Program, Memorial Sloan Kettering Cancer Center, New York, NY.

Etv6 (also known as TEL) is a member of the ETS family of transcription factors, which also includes important regulators of immune system development such as PU.1 (SPI1 or SFPI1), SPIB, and ETS1 (Hollenhorst et al., 2011). All ETS factors contain an ETS domain that mediates DNA binding to a consensus ETS-binding site, GGAA(gt). In addition, Etv6 and several other family members contain a Pointed (PNT) domain that mediates protein–protein interactions. Etv6 acts predominantly as a transcriptional repressor and is antagonized by other PNT-containing ETS proteins. In particular, reciprocal expression and functional antagonism of Etv6 and Ets1 have been reported in *Drosophila melanogaster* development for the respective orthologues Yan and Pointed (Graham et al., 2010; Boisclair Lachance et al., 2014) and in the differentiation of $CD4^+$ effector T cells (Liu et al., 2016). Etv6 is prominently expressed in hematopoietic stem and progenitor cells (HSPCs) and is essential for HSPC maintenance and thrombopoiesis (Hock et al., 2004; Hock and Shimamura, 2017). Moreover, chromosomal translocations encoding ETV6-containing fusion proteins, as well as monoallelic loss-of-function mutations of ETV6, are common in several types of leukemia (Hock and Shimamura, 2017). Thus, Etv6 is a key regulator of HSPC function and leukemogenesis, whereas its role in the differentiation of mature immune cell types has not been fully explored.

Here, we show that Etv6 is expressed in cDCs in the absence of its antagonist, Ets1, and is required for optimal differentiation of the cDC1 subset. In particular, Etv6-deficient cDC1 had an aberrant expression profile with up-regulation of pDC signature and showed deficient cross-priming of tumor-specific T cell responses. These results define Etv6 as a novel cell-intrinsic regulator of DC functionality that promotes cDC1-induced T cell responses.

Results and discussion

Etv6 is expressed in DCs and facilitates DC development in vitro

Genome-wide expression datasets such as Immgen (Heng et al., 2008; Miller et al., 2012) revealed the expected expression of Etv6 in murine HSPC, including all multipotent and lineage-committed progenitors such as common DC progenitors (CDPs; Fig. 1 A and data not shown). Among mature lineages, however, Etv6 was expressed primarily in DCs and monocytes (Fig. 1 A). Global mRNA sequencing (RNA-seq) of murine splenic DC subsets including pDC, cDC1 and cDC2 (the latter including the Notch-dependent $Esam^{hi}$ and the monocyte-like $Esam^{lo}$ subsets; Lewis et al., 2011) confirmed the expression of Etv6 in all these populations (Fig. 1 B). In contrast, Etv6 antagonist Ets1 is prominently expressed in lymphocytes, pDCs, and neutrophils but absent in HSPCs, cDCs and monocytes (Fig. 1, A and B). Another PNT domain–containing Ets factor, Ehf, is expressed in cDC2 but is low in cDC1 and absent in pDCs (Fig. 1 B). A similar expression pattern of Etv6 that is reciprocal to Ets1 is also observed in expression datasets of human cells such as the Primary Cell Atlas (Mabbott et al., 2013). A close Ets1 homologue, Ets2, is also expressed in human monocytes and cDC2, but not cDC1 (data not shown). Thus, in addition to the expected expression of Etv6 in HSPCs, it is also expressed in murine and human DCs. Furthermore, Etv6 is expressed in cDC1 in the absence of other PNT domain–containing Ets proteins, whereas the latter are expressed in pDCs (Ets1) and cDC2 (Ehf in mice and Ets2 in humans).

To test the potential function of Etv6 in DCs, we examined FLT3L-driven DC development from bone marrow (BM) cells in vitro. Because the germline Etv6 deletion is embryonic lethal and the constitutive Etv6 deletion causes HSPC depletion (Hock et al., 2004), we used the conditional null allele of *Etv6* ($Etv6^{flox}$) in combination with tamoxifen-inducible Cre recombinase ($R26^{CreER}$). The $Etv6^{flox/flox}$ $R26^{CreER/+}$ mice or WT controls (either $Etv6^{+/+}$ $R26^{CreER/+}$ or $Etv6^{flox/flox}$ $R26^{+/+}$) were treated with tamoxifen, causing the recombination of $Etv6^{flox}$ into the null $Etv6^{\Delta}$ allele as confirmed by genomic PCR (data not shown). At the early stages after tamoxifen treatment (days 7–9), the BM of globally deleted R26-$Etv6^{\Delta}$ mice showed only a slight reduction in overall cellularity (Fig. S1 A) and normal fractions of HSPCs, including myeloid progenitors and CDPs (Fig. S1 B). FLT3L-supplemented cultures of R26-$Etv6^{\Delta}$ BM contained reduced fractions and absolute numbers of $CD24^+$ $CD11b^{lo}$ cDC1-like cells (Naik et al., 2005; Fig. 1, C and D). The fractions of $CD24^-$ $CD11b^{hi}$ cDC2 or pDCs were not reduced, although a decrease of absolute pDC numbers was noted (Fig. 1, C and D). Similarly, mixed cultures with $CD45.1^+$ WT competitor BM cells revealed a significant reduction in the fraction of cDC1 from R26-$Etv6^{\Delta}$ BM ($CD45.2^+$) compared with control $CD45.2^+$ BM, whereas no significant change was observed in pDCs or cDC2 (Fig. 1 E).

Whereas FLT3L cultures of murine BM yield only $CD24^+$ $CD11b^{lo}$ $CD8\alpha^-$ cDC1-like cells, co-culture with Notch ligand–expressing OP9-DL1 cells generates fully differentiated $CD24^+$ $CD11b^-$ $CD8\alpha^+$ cDC1 (Kirkling et al., 2018). These co-cultures of R26-$Etv6^{\Delta}$ BM yielded a reduced fraction of $CD24^+$ $CD11b^-$ cDC1 and a profound loss of $CD8\alpha^+$ cells in the resulting DC population (Fig. 1 F). Collectively, these data suggest that the loss of Etv6 in the BM progenitors impairs FLT3L-driven in vitro differentiation of cDC1.

Etv6 facilitates optimal cDC1 differentiation in vivo

We analyzed mature DC populations after the tamoxifen-induced global deletion of Etv6 in R26-$Etv6^{\Delta}$ mice. The pDC population was reduced approximately twofold in the BM but remained normal in the spleen (Fig. 2, A and B). The reduction in the BM is consistent with a mild reduction of pDC numbers in vitro (Fig. 1 D) and may originate at the level of DC progenitors such as CDP, which express Etv6 but not Ets1. Within the cDC population, the numbers of splenic $CD11b^+$ cDC2 (both the $Esam^{hi}$ and $Esam^{lo}$ subsets) were unaffected, although a consistent increase in CD11b expression was noted (Fig. 2, C and D; and data not shown). The fraction and absolute numbers of splenic $CD11b^-$ $Dec205^+$ cDC1 were reduced ∼1.5-fold (Fig. 2, C and D). Furthermore, the remaining cDC1 cells showed a striking loss of CD8α expression (Fig. 2 E), consistent with the inability to generate $CD8\alpha^+$ cDC1 in vitro (Fig. 1 F). Other specific markers of cDC1, including CD24, Clec9a, and Xcr1, were expressed at normal levels (Fig. S1 C), and the overall distribution of $Dec205^+$ cDC1 within the spleen was unaffected (Fig. S1 D). The fractions of resident $CD8\alpha^+$ cDC1 and migratory $CD103^+$ cDC1 were unchanged in the skin draining lymph nodes (dLNs) and reduced approximately twofold in

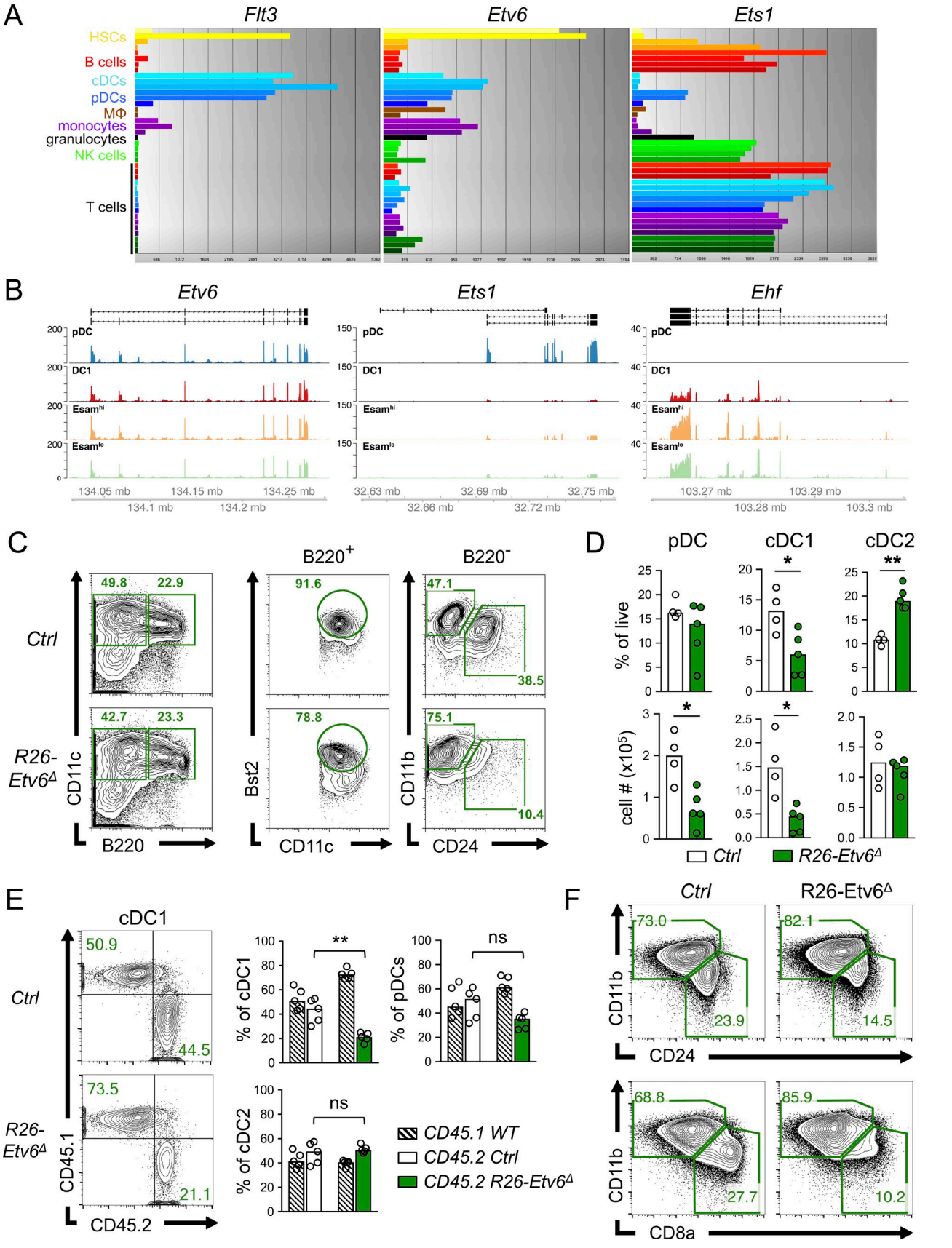

Figure 1. ***Etv6* is expressed in DCs and facilitates their development in vitro. (A)** The expression of *Etv6* in murine immune cell types. Shown are the expression profiles of *Flt3*, *Etv6*, and *Ets1* in the ImmGen microarray expression database of key immune populations. HSC, hematopoietic stem cell; Mφ, macrophage; NK, natural killer. **(B)** The expression of *Etv6* in murine splenic DC subsets as determined by RNA-seq. Shown are representative normalized counts mapped to

the mesenteric lymph nodes (Fig. S1, E and F). Furthermore, the fractions of CD103$^+$ cDC1 were unchanged in the lung (Fig. S1, E and F) and small intestine (data not shown). On the other hand, the expression of CD8α on resident cDC1 in all lymph nodes was strongly reduced (Fig. S1 G).

To test the consequences of cell-type–specific loss of Etv6, we used the DC-specific *Itgax*-Cre deleter strain (Caton et al., 2007). Because the efficiency of *Etv6*^{flox} allele recombination by *Itgax*-Cre was relatively low (data not shown), we used one conditional and one germline null allele of Etv6 (*Etv6*$^{flox/Δ}$ *Itgax*-Cre$^+$). The resulting mice with DC-specific Etv6 deletion (DC-*Etv6*^{Δ}) showed no hematopoietic abnormalities at any age. Similar to R26-*Etv6*^{Δ} mice, the pDC population was decreased in the BM, but not spleen (Fig. 2 B). The population of cDC1 was not significantly decreased in DC-*Etv6*^{Δ} spleens, likely reflecting a late onset of Cre recombination in the differentiating cDCs (Fig. 2 D). Nevertheless, a similarly profound loss of CD8α expression in cDC1 was observed (Fig. 2 F). Thus, Etv6 facilitates (but is not strictly required for) cDC1 differentiation in vivo and specifically controls the acquisition of CD8α expression.

Etv6 optimizes the gene expression profile and chromatin landscape of cDC1

Given the observed phenotypic alterations in cDC1, we asked how Etv6 deficiency affects the global expression profile of DCs. We established BM chimeras from DC-*Etv6*^{Δ} and WT control mice, sorted primary splenic DCs (including pDCs, cDC1, and the two cDC2 subsets), and analyzed them by RNA-seq (Tables S1, S2, S3, and S4). All Etv6-deficient samples showed a near-complete loss of sequence reads mapping to the deleted *Etv6* exons (data not shown). Principal-component analysis of all samples revealed that Etv6-deficient DC subsets maintained their overall identity and clustered closely with their WT counterparts, although some divergence in cDC1 was notable (Fig. 3 A). Pairwise comparisons within subsets confirmed the greatest differential expression in Etv6-deficient cDC1 (Fig. 3 B). Etv6-deficient pDCs were also affected, showing primarily gene up-regulation, whereas cDC2 showed minimal changes (Fig. 3 B). Next, we asked how the loss of Etv6 affected subset-specific expression programs in primary DCs. We used WT DC subsets to derive transcriptional signatures specific to cDC1, cDC2, all cDCs (i.e., cDC1 + cDC2), and pDCs (Fig. S2 A and Table S5). These signatures included genes encoding the key surface markers and transcription factors specific for the respective DC subsets (Fig. S2 A). We then tested the expression of these gene signatures in Etv6-deficient versus WT DCs using generally applicable gene set enrichment analysis (GAGE). We found that among genes that were down-regulated in Etv6-deficient cDC1 cells, there was a significant enrichment in cDC1 and cDC signature genes (Fig. 3 C). Conversely, among genes that were up-regulated in Etv6-deficient cDC1, there was a significant enrichment in the pDC signature genes (Fig. 3 C). For instance, Etv6-deficient cDC1 showed the expected down-regulation of *CD8a* as well as of other cDC1-specific genes, such as *Notch4* and *Gclc*, and up-regulation of pDC-specific genes, such as *Runx2* and *Cox6a2* (Fig. 3 D). A less significant up-regulation of pDC signature was also observed in cDC2 (Fig. 3 C). On the other hand, among genes that were up-regulated in Etv6-deficient pDCs, there was a significant enrichment in cDC signature genes (Fig. 3 C). Thus, Etv6 deficiency produced a partial impairment of subset-specific expression programs in cDC1 and to a lesser extent in pDCs.

IRF8 is critical for cDC1 development as well as for the development and/or function of pDCs. Etv6 was shown to interact with IRF8 and corepress select IRF8 target genes in IFN-treated macrophages (Kuwata et al., 2002) and in Th9 effector T cells (Humblin et al., 2017). Similarly, IRF8 and Etv6 could be coimmunoprecipitated from total DCs or enriched cDC1 from BM cultures (data not shown). The transcriptional targets of IRF8 in cDC1 have not been well defined, because the deletion of IRF8 at any point completely abolishes cDC1 differentiation (Sichien et al., 2016). To circumvent this limitation, we used genes affected by the deletion of IRF8 in the closest cell type, the pDC (Sichien et al., 2016), and defined gene sets that are up-regulated (IRF8.up) or down-regulated (IRF8.down) in IRF8-deficient splenic pDCs (Tables S1, S2, S3, and S4). Notably, we observed highly significant overlaps between the IRF8.up gene set and genes up-regulated in Etv6-deficient cDC1 and pDCs but only minimal overlaps in cDC2 (Fig. 3, E and F). Conversely, the IRF8.down gene set was not significantly enriched among down-regulated genes in any Etv6-deficient DC subset (Fig. 3, E and F). These data suggest that, as in other cell types, ETV6 may cooperate with IRF8 in the repression of its target genes in IRF8-expressing DC subsets.

To examine the effect of Etv6 on global chromatin accessibility, we analyzed DCs from DC-*Etv6*^{Δ} and control BM chimeras using the assay for transposase-accessible chromatin with sequencing (ATAC-seq; Tables S6, S7, and S8). As with the transcriptional profiling, we first used ATAC-seq profiles of WT DCs to derive chromatin signatures specific for each DC subset (Fig. S2 B and Table S9). De novo motif analysis of peak regions from DC chromatin signatures matched several motifs of known sub-

the *Etv6*, *Ets1*, and *Ehf* loci within the indicated DC subsets. **(C)** DC development in FLT3L-supplemented BM cultures from control (Ctrl) and *R26-Etv6*^{Δ} animals. Shown are representative staining plots of total day 7 cultures (left panel) and of gated CD11c$^+$ DC populations (right panels), highlighting B220$^+$ Bst2$^+$ pDCs, B220$^-$ CD11b^{hi} CD24$^-$ cDC2 and B220$^-$ CD11b^{lo} CD24$^+$ cDC1-like cells. **(D)** Frequencies among total live cells and absolute numbers of DC subsets shown in panel C. Shown are cultures from individual animals (n = 4–5) pooled from two experiments; bar represents the median. Statistical significance by Mann–Whitney test (*, P ≤ 0.05; **, P ≤ 0.01). **(E)** DC development in competitive FLT3L-supplemented BM cultures. CD45.2 control (Ctrl) or *R26-Etv6*^{Δ} BM cells were mixed 1:1 with CD45.1 WT competitor BM cells and cultured in the presence of FLT3L. Shown is representative staining of the gated cDC1-like population for donor and competitor cells and the frequencies of donor and competitor cells among the indicated DC subsets. Shown are cultures from individual animals (n = 5) pooled from two experiments; bar represents the median. Statistical significance by Mann–Whitney test (**, P ≤ 0.01; ns, not significant). **(F)** DC development in Notch-driven BM cultures. Total BM cells from control (Ctrl) and *R26-Etv6*^{Δ} animals were cultured for 7 d with FLT3L and OP9 stromal cells expressing the Notch ligand DL1 (OP9-DL1). Shown are representative staining plots of gated CD11c$^+$ MHCII$^+$ highlighting CD11b$^+$ CD24$^-$ CD8α$^-$ cDC2 and CD11b$^-$ CD24$^+$ CD8α$^+$ cDC1. Data are representative of two experiments.

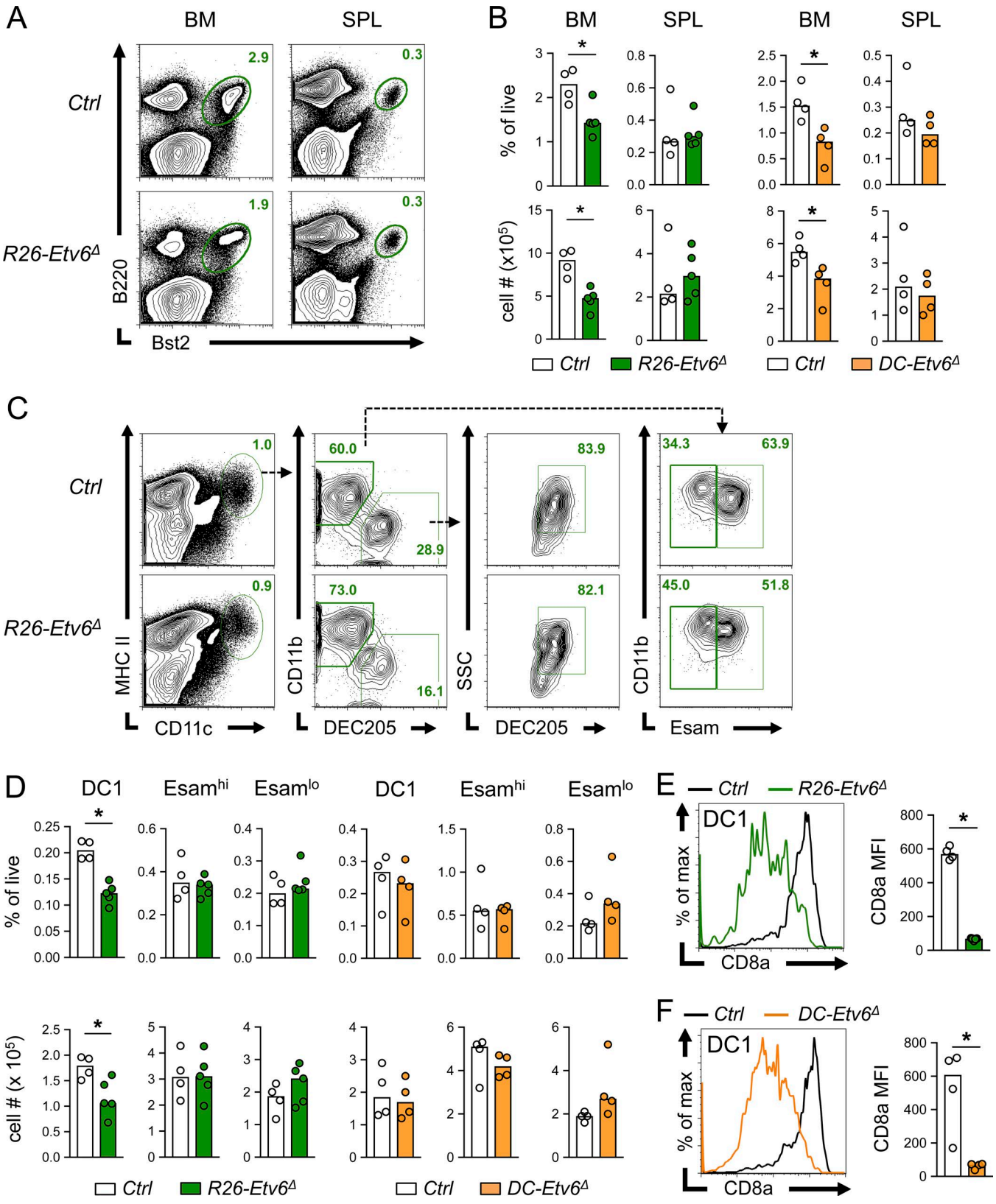

Figure 2. **Loss of *Etv6* impairs optimal cDC1 differentiation in vivo. (A–D)** Flow cytometry analysis of BM and splenic DC populations from control and *R26-Etv6*$^{\Delta}$ animals 9 d after tamoxifen treatment (green symbols), or from DC-*Etv6*$^{\Delta}$ (*Etv6*$^{flox/-}$ *Itgax*-Cre^{+}) and littermate control animals (orange symbols). Shown are individual values (n = 4–5) pooled from two experiments; bar represents the median. Statistical significance by Mann–Whitney test (*, P ≤ 0.05). **(A)** Representative staining plots with the fraction of B220^{+} Bst2^{+} pDCs in BM and spleen (SPL) indicated. **(B)** The frequencies among total live cells and absolute numbers of pDCs in BM and spleen (SPL). **(C)** Representative staining plots showing CD11c^{hi} MHCII^{+} cDCs and their subsets, including DEC205^{+} SSC^{hi} cDC1 and CD11b^{+} Esam^{hi} or Esam^{lo} cDC2. **(D)** Frequencies among total splenocytes and absolute numbers of DC subsets shown in panel C. **(E and F)** Expression of CD8α

set-specific transcriptional regulators of the respective subsets, including IRF/BATF motifs in the cDC1 signature and E-protein and Runx2 motifs in the pDC signature (Fig. S2 C). Notably, the canonical ETS-binding motif (designated as Sfpi1 motif) was among the top motifs enriched in the cDC signature (Fig. S2 C). Whereas the transcriptional signatures of DC subsets were comparable in size (Fig. S2 A), chromatin signatures were unequal (Fig. S2, B and D). Thus, pDCs and cDCs showed large chromatin signatures (>4,500 genes) that incorporated a sizable fraction of transcriptional signatures (54% and 45% of pDC-specific and cDC-specific genes, respectively; Fig. S2 D and Table S9). In contrast, cDC1- and cDC2-specific chromatin signatures were smaller (<1,500 genes) and showed little overlap with transcriptional signatures (21% and 11%, respectively), suggesting that cDC1/cDC2 subset specification does not involve extensive chromatin remodeling.

Among DC subsets, Etv6-deficient cDC1 showed the most prominent changes in chromatin signatures: the cDC signature was enriched among peaks that became less accessible, whereas the pDC signature was enriched among peaks that became more accessible (Fig. 4, A and B). This was also true for peaks assigned to genes that overlapped with the corresponding transcriptional signature genes (Fig. 4 C). A reciprocal pattern was observed in Etv6-deficient pDCs, albeit with a lower magnitude (Fig. 4, A and B). Thus, similar to the expression profiles, Etv6 deficiency caused a partial impairment in the subset-specific chromatin profile of cDC1.

We defined IRF8-bound genomic regions using chromatin immunoprecipitation (ChIP) data from in vitro–generated DCs (Grajales-Reyes et al., 2015; Table S9) and examined the accessibility of these IRF8-bound regions in the absence of Etv6. The deletion of Etv6 in cDC1 resulted in a coordinated increase in accessibility among Irf8-bound regions within the pDC signature (Fig. 4 D). For example, an intergenic region downstream of the *Pten* locus harbors a pDC-specific IRF8 target peak that became accessible in Etv6-deficient cDC1 (Fig. 4 E). Conversely, Etv6-deficient pDCs showed a significant increase in accessibility among IRF8-bound cDC signature regions (Fig. 4 D). This pattern is exemplified by a cDC intronic region of the *Deptor* locus that becomes more accessible in Etv6-deficient pDCs (Fig. 4 E). Furthermore, we observed an intronic region within the *Etv6* locus itself that is bound by IRF8 and loses accessibility specifically in cDC1 upon Etv6 deletion, suggesting upstream regulation of Etv6 by IRF8 (Fig. 4 E). Collectively, our results suggest that Etv6 fine-tunes the subset-specific expression and chromatin profiles of cDC1 and pDCs. In particular, Etv6 contributes to the repression of IRF8 target genes and antagonizes the inappropriate pDC-specific expression program in cDC1.

Etv6 facilitates T cell cross-priming and tumor antigen–specific responses

Given the aberrations in subset-specific gene expression in Etv6-deficient pDCs and cDC1, we analyzed the functions of these cells in R26-*Etv6*$^{\Delta}$ and DC-*Etv6*$^{\Delta}$ mice. Systemic production of IFN-α in response to TLR9 ligand CpG, a canonical pDC-mediated response, showed a modest (approximately twofold) decrease in R26-*Etv6*$^{\Delta}$ mice (Fig. S3 A). The production of IL-12 is a distinct property of cDC1 in response to pathogens such as *Toxoplasma gondii* or its extract (soluble tachyzoite antigen [STAg]; Reis e Sousa et al., 1997), which contains TLR11 ligand profilin (Yarovinsky et al., 2005). When assessed by ELISA, the STAg-induced production of IL-12 p70 protein was normal in R26-*Etv6*$^{\Delta}$ mice in vivo (Fig. S3 B). We also used the Luminex assay to measure the production of 10 cytokines in the serum of STAg-induced animals or supernatants of enriched splenic DCs incubated with profilin. In both cases, we observed a comparably strong induction of IL-12 p40/p70, IL-1β, IL-4, IL-6, IFN-γ, and GM-CSF, except for a minor (~25%) reduction of IL-12 in the supernatants of cultured R26-*Etv6*$^{\Delta}$ DCs (Fig. S3, C and D). The induction of IL-2, IL-5, and TNF-α was weaker but similarly comparable between control and R26-*Etv6*$^{\Delta}$ samples, whereas IL-10 was undetectable (data not shown). Thus, the loss of Etv6 does not affect the cytokine-producing capacity of cDC1 in vivo or in vitro.

We then tested the antigen-presenting capacity of Etv6-deficient DCs in vivo. Immunization with H-2K^{b}-restricted immunodominant OVA peptide induced the expansion of endogenous OVA-specific CD8^{+} T cells (stained with tetramers of H-2K^{b}–OVA peptide complexes) to the same extent in control and DC-*Etv6*$^{\Delta}$ animals (Fig. 5, A and B). To test cross-priming of CD8^{+} T cell responses to an exogenous cell-associated antigen, we injected allogeneic (H-2K^{q}) splenocytes loaded with OVA protein. The resulting expansion of OVA-specific CD8^{+} T cells was fully dependent on endogenous cDC1, because it was abolished in Batf3-deficient mice that specifically lack this subset (Fig. S3 E). In contrast to peptide immunization, the cross-priming of OVA-specific CD8^{+} T cells by cell-associated OVA was impaired in DC-*Etv6*$^{\Delta}$ mice (Fig. 5, C and D). By comparison, no impairment was observed in mice deficient for Mycl1, a transcription factor that was proposed to regulate peripheral homeostasis of cDC1 (Kc et al., 2014; Fig. S3, F and G). Thus, Etv6 expression in DCs facilitates optimal cDC1-mediated T cell cross-priming in vivo.

We examined endogenous tumor-specific CD8^{+} T cell responses by challenging mice subcutaneously (s.c.) with B16 melanoma cells expressing OVA (B16-OVA). The growth of B16-OVA cells was comparable between control and DC-*Etv6*$^{\Delta}$ mice, resulting in skin tumors of similar size (data not shown). Compared with the challenge with OVA-negative parental B16 cells, challenge with B16-OVA caused an expansion of activated OVA-specific CD44^{+} CD8^{+} T cells in the tumor dLNs (Fig. 5, E and F). Importantly, this expansion was significantly reduced in DC-*Etv6*$^{\Delta}$ mice (Fig. 5, E and F). To test the functional consequences of impaired tumor-specific T cell responses, we used injection of MC38 adenocarcinoma cell line with or without the T cell checkpoint blockade with anti-CD137 (4-1BB). The response of MC38-derived tumors to anti-CD137 was shown to require cDC1, as it was abolished in Batf3-deficient animals (Sánchez-Paulete et al., 2016). Indeed, anti-CD137 reduced

on the splenic cDC1 population gated as shown in panel C. Shown are representative histograms and mean fluorescence intensity (MFI) of CD8α in cDC1 from individual mice (n = 4–5) pooled from two experiments; bars represent median. Statistical significance by Mann–Whitney test (*, P ≤ 0.05). **(E)** Global Etv6 deletion in *R26-Etv6*$^{\Delta}$ animals 9 d after tamoxifen treatment. **(F)** DC-specific Etv6 deletion in DC-*Etv6*$^{\Delta}$ (*Etv6*$^{flox/-}$ *Itgax*-Cre^{+}) animals.

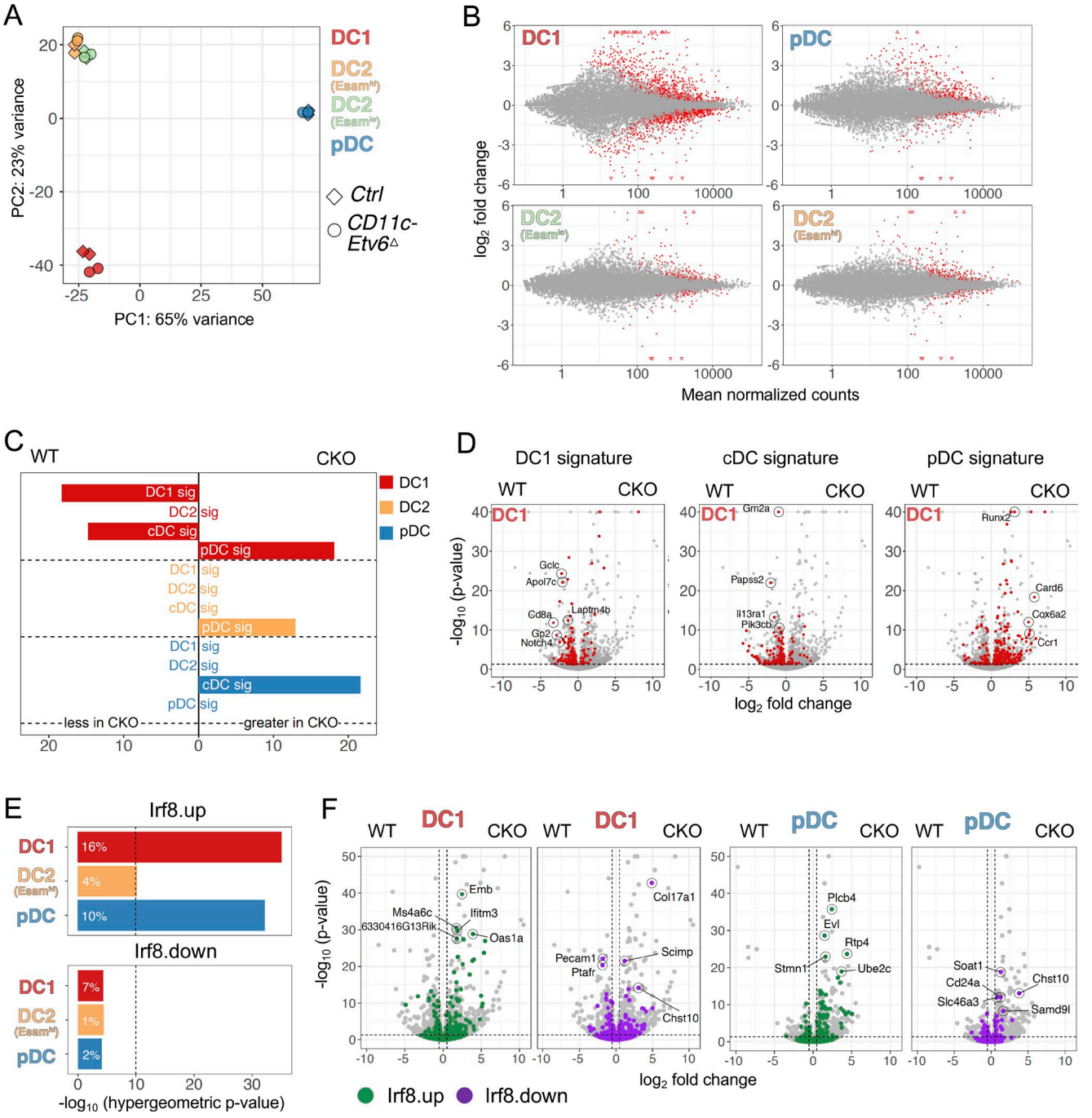

Figure 3. **Loss of *Etv6* impairs subset-specific expression profiles of DCs.** Primary splenic DC subsets (pDC, cDC1, Esam^{hi}, and Esam^{lo} cDC2) were sorted from individual chimeric mice reconstituted with BM from DC-*Etv6*$^{\Delta}$ (conditional KO [CKO]) or control WT donors. The resulting cell populations were analyzed by RNA-seq; $n = 2$ per genotype. **(A)** Principal component (PC) analysis of expression profiles on the top 500 most variable genes. **(B)** Pairwise comparisons of expression profiles within each DC subset. x axis depicts average normalized counts across all samples, whereas the y axis depicts moderated $\log_2$FC of CKO over WT control. Red dots indicate differentially expressed genes ($p_{adj} < 0.05$), while red arrows indicate data points that lie beyond axis limits. **(C)** The enrichment of DC subset-specific transcriptional signatures in Etv6-deficient DCs. Shown are bar plots of $-\log_{10}$-transformed P values calculated from GAGE analysis of CKO versus WT control DC subsets including cDC1 (red), cDC2 (yellow), or pDCs (blue). Each subset was tested for cDC1, cDC2, cDC, and pDC signatures as indicated. Direction of bar plots indicates whether enrichment was found in up-regulated (greater in CKO, right) or down-regulated (greater in WT, left) genes for each DC subset. **(D)** Volcano plots of differential expression between CKO and control cDC1. x axis depicts fold change (moderated $\log_2$FC), while y axis depicts significance ($-\log_{10}$-transformed false discovery rate–adjusted P values). Red dots show differentially expressed genes ($p_{adj} < 0.05$) that are a part of the indicated transcriptional signatures. **(E)** The enrichment of IRF8-regulated targets among Etv6-regulated genes. Bar plots depict hypergeometric P value calculated for commonly up-regulated (IRF8.up) or down-regulated (IRF8.down) genes in IRF8-deficient pDCs and indicated Etv6-deficient DC subsets ($p_{adj} < 0.05$; $|\log_2 FC| > 0.5$). All expressed genes from DC subsets, including all IRF8 targets, were used as background. Vertical line indicates the P value cutoff of 10^{-10}. Percentages indicate proportion of common genes out of total up-regulated (735) or down-regulated (828) IRF8 targets. **(F)** Volcano plots of differential expression between *Etv6* CKO and control cDC1 and pDC. Green dots mark genes that are up-regulated (IRF8.up) and purple dots mark those that are down-regulated (IRF8.down) in IRF8-deficient pDCs. Circles highlight the top five most significant IRF8 targets, ranked by p_{adj}. Vertical line represents $\log_2$FC ±0.5, while horizontal line indicates false discovery rate–adjusted P value of 0.05.

the median tumor size and increased survival in MC38-challenged control mice, but these effects were abolished in DC-*Etv6*$^{\Delta}$ mice (Fig. S3, H and I). Although small group sizes precluded statistical significance, these results show a trend toward reduced control of tumor growth by Etv6-deficient DC1. Collectively, these data demonstrate that Etv6 expression in DCs facilitates CD8$^+$ T cell cross-priming and tumor-specific responses.

We describe a new role of the transcriptional repressor Etv6, a well-known regulator of HSPC maintenance and leukemogenesis, in the differentiation and function of cross-presenting cDC1 cells. This cell type–specific role likely reflects the expression of Etv6 in the absence of its ETS family antagonists such as Ets1 or related factors, as well as its synergistic activity with IRF8. Etv6 deletion reduced cDC1 development (especially in vitro) but, unlike the loss of IRF8 or BATF3, did not abolish it. The phenotype could not be rescued by Notch signaling, suggesting that Etv6 acts upstream of or parallel to Notch. Notably, Etv6 deletion reduced a subset of cDC1-specific genes (including the signature phenotypic marker CD8α) and caused a partial de-repression of IRF8-repressed genes and of the pDC expression signature. A converse, albeit weaker effect was observed in pDCs, where Etv6 deletion caused inappropriate induction of certain cDC-specific genes. These effects were mirrored by similar changes in chromatin signatures, although the latter largely discriminate between pDCs and cDCs, but not between cDC1/cDC2 subsets. Thus, Etv6 appears to act in committed cDC1 downstream of IRF8 and Batf3 (but upstream of Notch2), cooperating with IRF8 to refine the cDC1-specific gene expression profile. In particular, Etv6 may help "resolve" the expression profiles of cDC1 and pDCs, further emphasizing the close genetic similarity of the two DC types.

At the functional level, the loss of Etv6 impaired cDC1-dependent T cell cross-priming in vivo. Whereas negative transcriptional regulators of cross-presentation such as TFEB have been identified (Samie and Cresswell, 2015), factors that elicit this unique capacity in cDC1 remain unknown. Transcription factor Mycl1 was proposed to promote peripheral cDC1 homeostasis (Kc et al., 2014), yet we found it dispensable for cross-priming against cell-associated antigens. Thus, Etv6 represents a novel type of transcriptional regulator that is dispensable for the development of cDC1 but controls their signature functional property (i.e., their ability to cross-prime CD8$^+$ T cells). Accordingly, DC-specific deletion of Etv6 did not affect DC numbers but impaired T cell cross-priming against a model tumor-associated antigen and impaired the cDC1-dependent inhibition of tumor growth by checkpoint blockade. These results emphasize the cross-priming capacity of cDC1 as an essential DC function in tumor-specific responses and establish a novel animal model for its study toward translational applications for tumor immunotherapy.

Materials and methods

Animals

All animal studies were performed according to the investigator's protocol approved by the Institutional Animal Care and Use Committees of Columbia University or New York University School of Medicine. *Etv6*$^{flox/flox}$ mice (Hock et al., 2004) were crossed to *R26*^{CreER} (de Luca et al., 2005) or *Itgax*-Cre (Caton et al., 2007) deleter strains. All these strains have been backcrossed to C57BL/6 mice for >10 generations. For R26-*Etv6*$^{\Delta}$ (*Etv6*$^{flox/flox}$ *R26*$^{CreER/+}$) mice, either *Etv6*$^{+/+}$ *R26*$^{CreER/+}$ mice from the same colony or *Etv6*$^{flox/flox}$ *R26*$^{+/+}$ littermates were used as WT controls; no differences were noted in any measured parameter between these two types of controls. In the *Itgax*-Cre cross, a spontaneous germline recombination was used to generate the *Etv6*$^{\Delta}$ allele. For the resulting DC-*Etv6*$^{\Delta}$ (*Etv6*$^{\Delta/flox}$ *Itgax*-Cre$^+$), Cre-negative *Etv6*$^{flox/flox}$ or *Etv6*$^{+/flox}$ mice were used as controls. To establish chimeras, 2 × 10^6 whole BM cells harvested from either DC-*Etv6*$^{\Delta}$ (*Etv6*$^{\Delta/flox}$ *Itgax*-Cre$^+$) mice or Cre-negative *Etv6*$^{flox/flox}$ controls were transferred into lethally irradiated congenic B6.SJL recipients. Genotyping for the WT, conditional, and deleted Etv6 alleles was performed by PCR using the following primers: 5′-TTCCATGTGTTACCTCTGTCCG-3′, 5′-ACTGAACTGAGTTCTGCTGAG-3′, and 5′-ACCACACCAGTTGGTCATGAA-3′.

Batf3$^{-/-}$ mice on C57BL/6 background were purchased from the Jackson Laboratory (Hildner et al., 2008). *Mycl1*^{flox} mice on 129Sv background were obtained from the Jackson Laboratory (stock no. 013184) and bred to *Itgax-Cre* mice. WT C57BL/6, B6.SJL, BALB/c, and FVB mice were obtained from Taconic. Mice were group-housed in individually ventilated cages and maintained under specific pathogen–free conditions. Male and female mice were used between 8 and 20 wk of age. No obvious difference between sexes was observed within the parameters analyzed for our experiments.

Cell culture

The C57BL/6-derived B16 melanoma cell line (Mayordomo et al., 1995) and OVA-expressing (Falo et al., 1995) B16 clone (B16-OVA) were provided by H. Salmon and M. Merad (Icahn School of Medicine at Mount Sinai) and cultured in DMEM supplemented with 10% FCS, 1% L-glutamine, 1% sodium pyruvate, 1% MEM-NEAA, and 1% penicillin/streptomycin (full DMEM) at 37°C in a humidified atmosphere at 5% CO_2. The FLT3L-secreting clone of B16 (Mach et al., 2000) was used to produce FLT3L-containing supernatants and was cultured as above. The C57BL/6-derived MC38 colon adenocarcinoma cell line was provided by M. Vaeth and S. Feske (NYU School of Medicine) and cultured in full DMEM supplemented with 1% Hepes.

In vitro FLT3L-driven DC development

Primary BM cells were plated in a 24-well plate at a density of 2 × 10^6 cells per well, cultured in full DMEM supplemented with 10% supernatant from the cultured B16-FLT3L cell line, and harvested 7 d later. For competitive BM cultures, donor BM cells were mixed 1:1 with B6.SJL BM cells and cultured as above. Notch-driven BM cultures were initiated as above, and on day 3, the cells were harvested and co-cultured with OP9-DL1 cells as described previously (Kirkling et al., 2018). Cell co-cultures were analyzed on day 7.

Cell preparations

Lungs were perfused with 5 ml PBS via the right ventricle and lung dLNs were removed. Lungs and spleens were minced and digested with 1 mg/ml collagenase D and 20 µg/ml DNase I in full DMEM for 30–60 min at 37°C. Tissues were pressed through nylon

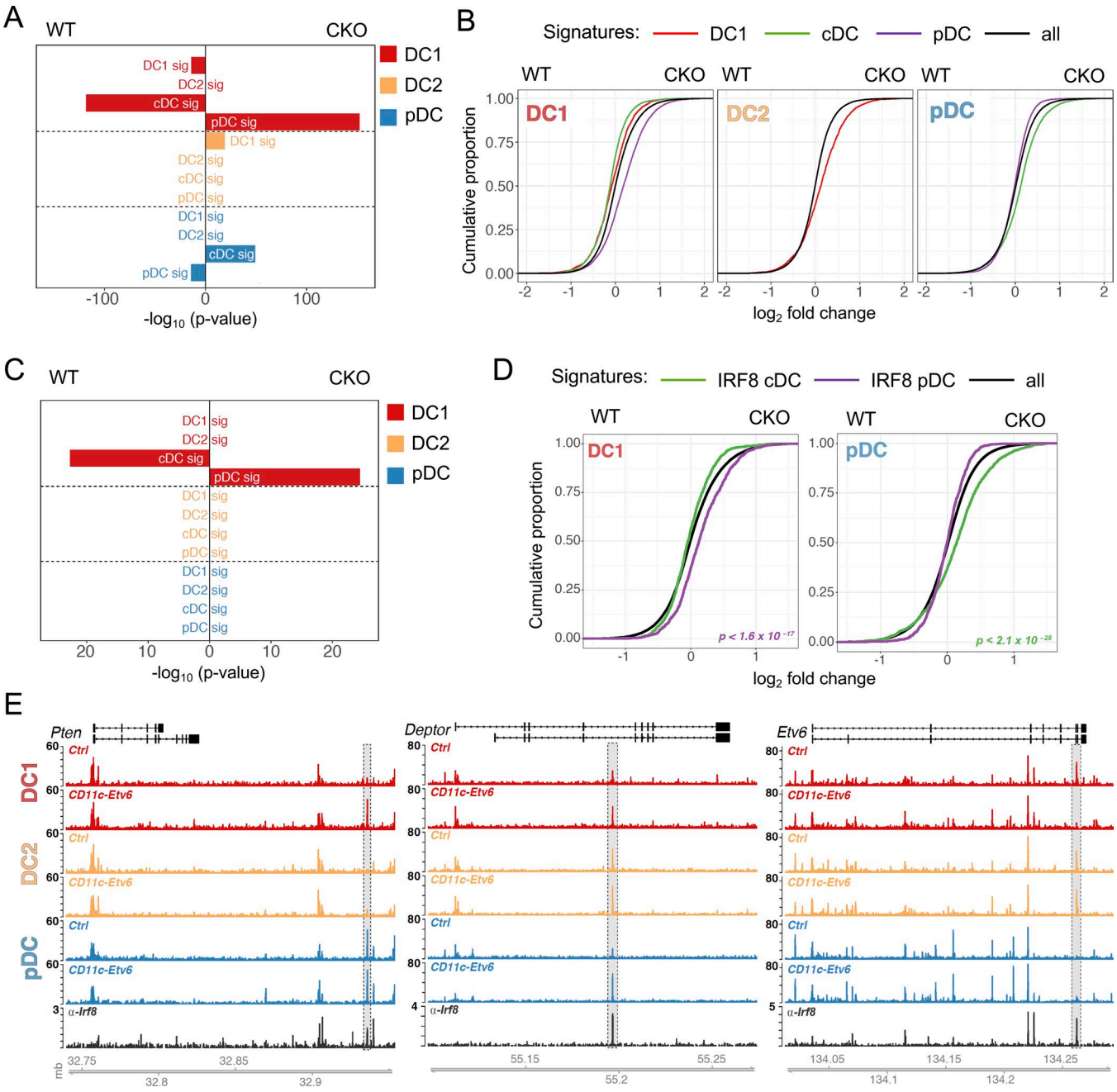

Figure 4. **Loss of *Etv6* impairs subset-specific epigenetic profiles of DCs.** Primary splenic DC subsets (pDC, cDC1, and cDC2) were sorted from individual chimeric mice reconstituted with BM from DC-*Etv6*$^{\Delta}$ (CKO) or control WT donors. The resulting cell populations were analyzed by ATAC-seq; $n = 2$ per genotype. **(A)** The enrichment of DC subset-specific chromatin signatures in Etv6-deficient DCs. Shown are bar plots of $-\log_{10}$-transformed P values calculated from GAGE analysis of CKO versus control DC subsets including cDC1 (red), cDC2 (yellow), or pDC (blue). Each subset was tested for cDC1, cDC2, cDC, and pDC signatures as indicated. Direction of bar plots indicates whether enrichment was found in up-regulated (greater in CKO, right) or down-regulated (less in CKO, left) peaks for each DC subset. **(B)** The accessibility of subset-specific chromatin signatures in Etv6-deficient DC subsets. Shown are cumulative distributions of differential accessibility ($\log_2$FC of peaks in CKO vs. control DCs) for all open regions (black) or for regions from signatures of cDC1 (red), cDCs (green) or pDCs (purple). **(C)** The enrichment in Etv6-deficient DCs of subset-specific chromatin signatures that also overlap with transcriptional signatures. Data are shown as in panel A. **(D)** The accessibility of IRF8-bound chromatin regions in Etv6-deficient DC subsets including cDC1 (left) and pDC (right). Shown are cumulative distributions of differential accessibility ($\log_2$FC of peaks in CKO vs. control DCs) for all accessible regions (black); cDC-specific IRF8-bound regions (green) and pDC-specific IRF8-bound regions (purple). P values were calculated using a one-sided Kolmogorov–Smirnov test comparing all log2FC to log2FC within each signature (indicated by color of text). **(E)** Representative ATAC-seq profiles highlighting regions of differential accessibility (light gray) in Etv6-deficient DC subsets. The y axis represents normalized read counts from ATAC-seq tracks and tags per million for the IRF8 ChIP track (dark gray, bottom), while the x axis represents genomic coordinates in megabases.

70-µm cell strainer to yield single-cell suspensions and then subjected to RBC lysis (155 mM NH_4Cl, 10 mM $NaHCO_3$, and 0.1 mM EDTA) for 5 min at room temperature before being filtered. BM was prepared by flushing femurs and tibias with PBS using a 27-gauge needle before RBC lysis. Lymph nodes were pressed through a 70-µm cell strainer to generate single-cell suspensions.

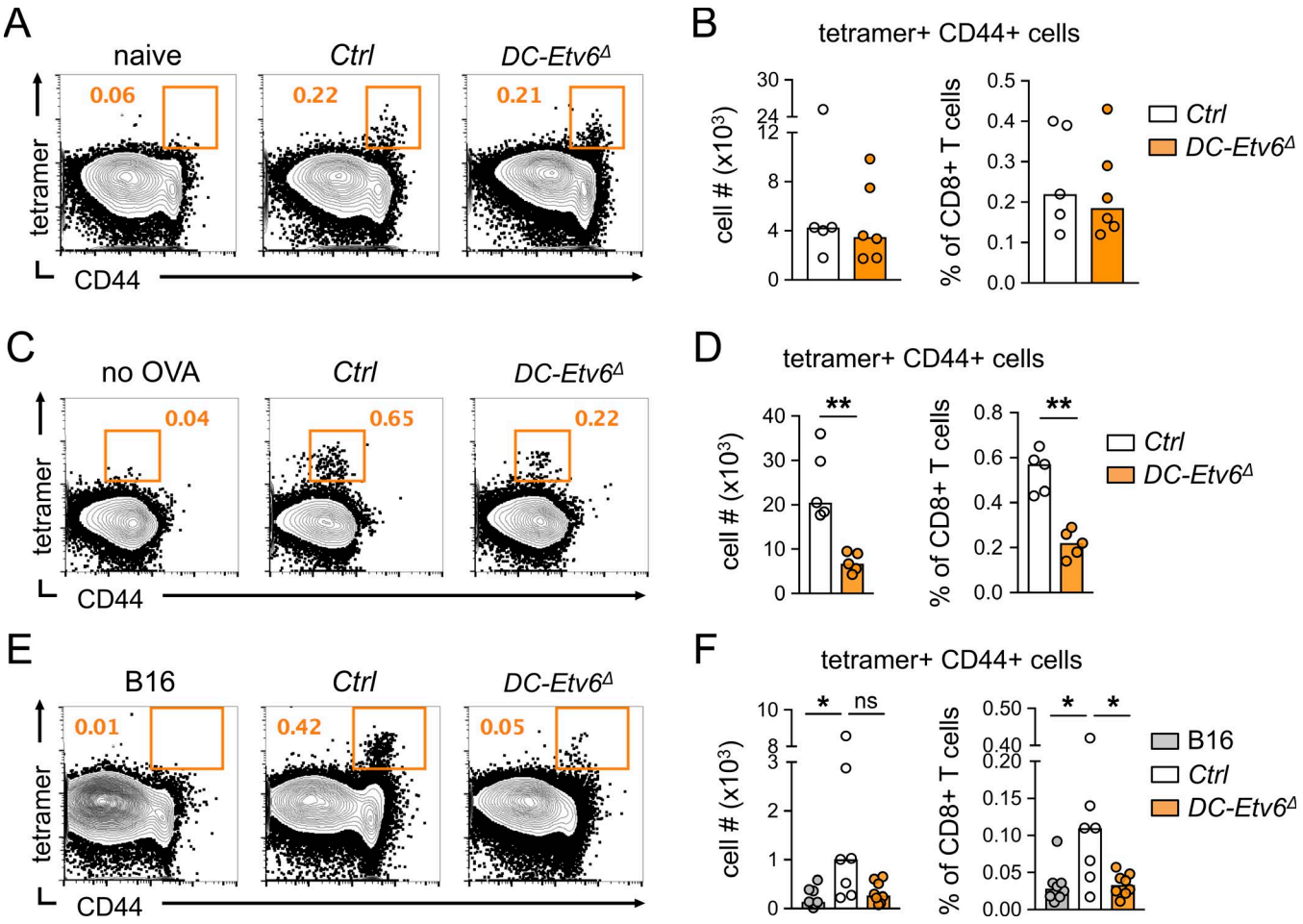

Figure 5. ***Etv6* deficiency in DCs leads to impaired T cell cross-priming and tumor antigen–specific responses. (A and B)** In vivo antigen-specific CD8⁺ T cell priming by peptide. DC-*Etv6*$^{\Delta}$ (*Etv6*$^{flox/-}$ *Itgax*-Cre) or control (*Etv6*$^{flox/flox}$) animals were immunized with $OVA_{257–264}$ peptide. 6 d after immunization, dLNs were harvested and analyzed for OVA-specific CD8⁺ T cells using OVA peptide/H-2K^{b} tetramer staining. **(A)** Representative staining plots of gated CD8⁺ T cells with the fraction of tetramer-positive cells indicated. **(B)** Absolute numbers of tetramer-positive cells and frequencies of tetramer-positive cells among total CD8⁺ T cells in dLNs. Shown are individual values of $n = 5$ from a single experiment; bars represent the median. **(C and D)** In vivo cross-priming of antigen-specific CD8⁺ T cells by allogeneic splenocytes. OVA-pulsed splenocytes from FVB mice (H-2^{q}) were injected i.v. into DC-*Etv6*$^{\Delta}$ (*Etv6*$^{flox/-}$ *Itgax*-Cre) or control (*Etv6*$^{flox/flox}$) animals. 7 d after the transfer, the spleens were harvested and analyzed for OVA-specific CD8⁺ T cells using OVA peptide/H-2K^{b} tetramer staining. **(C)** Representative staining plots of gated CD8⁺ T cells with the fraction of tetramer-positive cells indicated. **(D)** Absolute numbers of tetramer-positive cells and frequencies of tetramer-positive cells among total CD8⁺ T cells in the spleen. Shown are individual values of $n = 5$ mice from a single experiment; bars represent the median. Statistical significance by Mann–Whitney test (**, $P \le 0.01$). **(E and F)** In vivo cross-priming of CD8⁺ T cells specific for tumor-associated model antigen. DC-*Etv6*$^{\Delta}$ (*Etv6*$^{flox/-}$ *Itgax*-Cre) or control (*Etv6*$^{flox/flox}$) animals were inoculated with parental B16 melanoma cells (B16) or an OVA-expressing clone (B16-OVA). Tumor dLNs were harvested 16–17 d later and analyzed for OVA-specific CD8⁺ T cells using OVA peptide/H-2K^{b} tetramer staining. **(E)** Representative staining plots of gated CD8⁺ T cells with the fraction of tetramer-positive cells indicated. **(F)** Absolute numbers of tetramer-positive cells and frequencies of tetramer-positive cells among total CD8⁺ T cells in tumor dLNs. Shown are individual values of $n = 6–8$ pooled from three experiments; bars represent the median. Statistical significance by Mann–Whitney test (*, $P \le 0.05$).

Flow cytometry

Single-cell suspensions of splenocytes, BM, lung, or skin dLN cells were prepared as described above and stained for multicolor analysis with the indicated fluorochrome- or biotin-conjugated antibodies. For progenitor analysis, BM cells were stained with a cocktail of antibodies to lineage markers (B220, CD11b, CD11c, CD3 or TCRb, Ly6G, NK1.1, and Ter119). Staining of surface molecules with fluorescently labeled antibodies was performed for 20 min at 4°C in the dark. For in vivo cross-presentation assays and tumor induction experiments, the OVA peptide/H-2K^{b} tetramer was used and staining was performed for 30 min at room temperature. Samples were acquired on LSR II (BD) flow cytometer using FACSDiva software (BD Biosciences) or Attune NxT (Invitrogen) using Attune NxT software and further analyzed with FlowJo software.

Confocal microscopy

Spleens were harvested, fixed overnight at 4°C in 0.05 M phosphate buffer containing 0.1 M L-lysine, pH 7.4, 2 mg/ml NaIO4, and 1% PFA and dehydrated in 30% sucrose overnight at 4°C before embedding in OCT (optimal cutting temperature) compound. 20-µm-thick spleen sections were stained in PBS buffer containing 2% FBS, 0.05% Tween-20, and 0.3% Triton-X for 1 h at room temperature. Spleen sections were stained for CD11c (N418), DEC205 (205yekta), and TCRβ (H57-597). Con-

focal images were acquired using a Zeiss LSM 880 and analyzed using Bitplane's Imaris XT for colocalization and spot function rendition.

Tamoxifen treatment

To induce recombination in the Etv6$^{flox/flox}$ *R26*^{CreER} mice, animals were treated by oral gavage for three consecutive days with 5 mg of tamoxifen (Sigma Aldrich) suspended in sunflower seed oil. Mice were analyzed 9 d after the last treatment.

IFN assay

To induce an IFN response in vivo, *Etv6*$^{flox/flox}$ *R26*$^{CreER/+}$ or control mice were treated with tamoxifen as described above. 9 d after the last treatment, mice were injected intravenously with 5 µg of CpG-A (ODN 2216; InvivoGen) complexed with DOTAP (30 µl DOTAP/100 µl total volume; Roche), and blood was collected 6 h later by cardiac puncture. IFN-α concentration in the sera was determined by ELISA (LumiKine mIFN-α; InvivoGen) according to the manufacturer's recommendations.

In vivo T cell priming assay

Mice were immunized s.c. at the base of the tail with 100 µg $OVA_{257-264}$ (SIINFEKL; InvivoGen) emulsified in equal volume of CFA. dLNs were excised 6 d later and analyzed by flow cytometry using OVA peptide/H-2K^b tetramer staining.

In vivo cross-presentation assay

Chicken OVA protein (Sigma Aldrich) was hypertonically pulsed into FVB (H-2^q) or BALB/c (H-2^d) splenocytes. Briefly, cells were incubated with a hypertonic solution of 10% polyethylene glycol, 0.5 M sucrose, 10 mM Hepes, and 10 mg/ml OVA in RPMI buffer for 10 min at 37°C and then immediately flushed with a hypotonic solution of 40% water in RPMI. Cells were incubated for 2 min at 37°C and washed with cold PBS. Cells were irradiated with 2,000 cGy and injected into H-2^b mice at 4 × 10^7 cells per recipient. 7 d after the transfer, the spleens were harvested and analyzed by flow cytometry using OVA peptide/H-2K^b tetramer staining.

Tumor induction

Cultured tumor cells were collected before reaching confluence and washed twice with PBS. B16 parental or B16-OVA tumor cells (3 × 10^5) were injected s.c. in 100 µl PBS on the dorsal flank. Tumor growth was monitored and 16–17 d after injection tumor dLNs were harvested and analyzed by flow cytometry using OVA peptide/H-2K^b tetramer staining. MC38 tumor cells (5 × 10^5) were injected s.c. in 100 µl PBS on the dorsal flank. Anti-CD137 (LOB12.3) antibody was purchased by BioXCell and 100 µg was administered intraperitoneally in 100 µl PBS on days 4, 7, and 10 after tumor inoculation. Tumor growth was assessed by caliper.

STAg administration

The RH strain of *T. gondii* were propagated at 37°C by biweekly passage in human foreskin fibroblast cultures. STAg was prepared by sonication of RH parasites in the presence of protease inhibitors and centrifugation at 100,000 × *g*, and the supernatant was subsequently dialyzed against PBS (Yap et al., 1998). Mice were injected intraperitoneally with 20 or 25 µg STAg, and blood was acquired 6 h and 12 h later by tail bleeding and/or cardiac puncture. Blood was collected 1 d before vaccination by tail bleeding to determine the steady state. Cytokine levels in the sera were assessed by ELISA (mouse IL-12 p70 ELISA Ready-SET-Go; eBioscience) or Luminex multiplex assay.

In vitro activation assay

Spleens were processed as described, and DCs were then enriched by positive selection using biotinylated anti-CD11c, streptavidin microbeads, and MACS columns (Miltenyi Biotec) according to the manufacturer's recommendations. Splenic DCs were cultured in round-bottom, 96-well plates (5 × 10^5 cells/well) and stimulated with 100 ng/ml *T. gondii* profilin (Sigma Aldrich). Culture supernatants were collected 24 h later and cytokine levels were determined by Luminex multiplex assay.

Mouse cytokine multiplex assay

Sera and culture supernatants were collected as described above and immediately stored at −80°C. GM-CSF, IFN-γ, IL-1β, IL-2, IL-4, IL-5, IL-6, IL-10, IL-12 (p40/p70), and TNF-α levels in the samples were analyzed in a multiplex assay system (Cytokine Mouse Magnetic 10-plex Panel LMC0001M; Invitrogen). The assay was performed according to the manufacturer's instructions. Data were acquired on a MAGPIX instrument, and cytokine levels were quantitated using the xPONENT 4.2 software (Luminex).

Cell sorting and sample preparation for RNA-seq and ATAC-seq

Chimeras reconstituted with the BM of DC-*Etv6*^{Δ} (*Etv6*$^{flox/-}$ *Itgax*-Cre) or Cre-negative littermate controls (*Etv6*$^{flox/flox}$) were used as a source of cells. Splenic DCs were first enriched by positive selection using biotinylated anti-CD11c, streptavidin microbeads, and MACS columns (Miltenyi Biotec) and then sorted on either FACSAria (BD) or MoFlo (Beckman Coulter) instruments. CD45.2$^+$ DC populations were sorted as follows: pDC (Bst2$^+$ B220$^+$ CD11b$^-$); cDCs (CD11c^{hi} MHCII$^+$B220$^-$) and subsets thereof; cDC1 (Dec205$^+$ SSC^{hi}); and cDC2 (CD11b$^+$ Esam^{hi} and CD11b$^+$ Esam^{lo} separately for RNA, or bulk CD11b$^+$ for ATAC).

For RNA-seq, sorted cells (3–5 × 10^3) cells were resuspended in 750 µl TRIzol LS (Invitrogen) and stored at −80°C. RNA was extracted using the Arcturus PicoPure kit (Thermo Fisher Scientific). An equal volume of 70% ethanol was added to the aqueous phase of TRIzol samples and applied to columns from the PicoPure kit. Up to 250 µl of an ethanol/aqueous phase mix was loaded onto the column and spun at 100 *g* for 2 min for each load. Bound RNA was washed, treated with DNase I (QIAGEN), and eluted as per the manufacturer's instructions. To remove phenol contamination, the eluate was resuspended in 100 µl of wash buffer 1 and reloaded onto a fresh column followed by elution. cDNA libraries were prepared using the SMART-seq v4 Ultra Low Input RNA kit and Low Input Library Prep kit (Life Sciences), and single-end sequencing was performed in Illumina HiSeq 2500. For ATAC-seq, sorted cells (2 × 10^5) were washed with PBS and prepared as described previously (Buenrostro et al., 2015), and paired-end sequencing was performed in Illumina HiSeq 2500.

RNA-seq analysis

Single-end RNA-seq reads from all samples were trimmed to remove low-quality reads using Trimmomatic (v.0.36; Bolger et al., 2014). Trimmed reads were mapped to the *Mus musculus* genome (mm10 assembly) using Bowtie2 (v.2.2.9) and samtools (v.1.3.1; Li et al., 2009; Langmead and Salzberg, 2012). Reads were counted in exon regions using the summarizeOverlaps function within the GenomicAlignments package (v.1.10.1) based on the University of California, Santa Cruz (UCSC) mm10 knownGene model and annotation database (Lawrence et al., 2013; Speir et al., 2016). For RNA-seq analysis of IRF8-deficient pDCs, raw counts were obtained from the Gene Expression Omnibus (GSE85520), and gene names were matched to the UCSC mm10 knownGene nomenclature. Differential gene expression and normalized counts scaled for sequencing depth were calculated using DESeq2 (v.1.14.1; Love et al., 2014).

ATAC-seq analysis

Paired-end ATAC-seq reads from all samples were trimmed and aligned as with RNA-seq processing. All positive-strand reads were shifted 4 bp downstream and all negative-strand reads were shifted 5 bp upstream to center the reads on the transposon binding event. Shifted, concordantly aligned paired mates were used for peak calling by MACS2 (v.2.1.1.20160309; Zhang et al., 2008) at a P value threshold of 0.01. Irreproducible discovery rate calculations using Python3 scripts (v2.0.2) were performed on all pairs of replicates using an oracle peak list called from merged replicates (Li et al., 2011). A union of peaks passing a threshold of 0.05 was used as a reference peak list for read counts. Read counts were generated using the summarizeOverlaps function from the GenomicAlignments package by counting reads that fell within peak regions, and DESeq2 was used to calculate differential accessibility and normalized counts scaled for sequencing depth. A total of 59,703 accessible regions were identified. Gene tracks were generated by converting BAM files to bigwig files using bedtools2 (v.2.26.0) and UCSC's bedGraphToBigWig (v.4) and visualized using the Gviz R package (v.1.18.2; Kent et al., 2010; Quinlan and Hall, 2010; Hahne and Ivanek, 2016).

ChIP-seq analysis

Fastq files from Irf8 ChIP-seq performed on ex vivo–cultured $CD24^+$ DCs and pDCs (Grajales-Reyes et al., 2015) were downloaded from the EMBL-EBI repository. Reads were trimmed and aligned as above. Peak calling was performed by MACS2 using default parameters, and only peaks that had a −log10(q-value) >10 were considered as Irf8 bound.

Peak annotation

Peak assignment was done using ChipPeakAnno (v.3.8.9) using the UCSC knownGene model (Zhu et al., 2010). Promoter regions were defined as peaks that overlapped a region that was +2 kb to −0.5 kb from the transcription start site (TSS). Intragenic (intronic and exonic) peaks were defined as any peak that overlapped with annotated intronic and exonic peaks, respectively, based on the annotation database. Intergenic peaks were defined as any nonpromoter or nonintragenic peaks, and were assigned to the gene of the nearest TSS based on the distance from the start of the peak. Priority was given to transcripts that were canonical, based on the UCSC known Canonical database. If peaks were assigned to multiple transcripts that contained the same TSS, one was chosen arbitrarily.

Transcriptional and epigenetic signatures

Pairwise comparisons of all WT DC subsets was performed and DC signatures were defined as follows: cDC signature, features commonly up-regulated (Benjamini–Hochberg adjusted P value [padj] < 0.05; $\log_2$ fold change [$\log_2$FC] > 0.5) when comparing cDC1 versus pDC and cDC2 versus pDC but are not different (padj > 0.05 or $|\log_2 FC| < 0.5$) when comparing cDC1 versus cDC2; pDC signature, features commonly up-regulated (padj < 0.05; $\log_2$FC > 0.5) in pDCs when compared with cDC1 and when compared with cDC2; cDC1 signature, features commonly up-regulated (padj < 0.05; $\log_2$FC > 0.5) in cDC1 when compared with pDCs and when compared with cDC2, and is not a cDC feature; cDC2 signature, features commonly up-regulated (padj < 0.05; $\log_2$FC > 0.5) in cDC2 when compared with pDCs and when compared with cDC1, and is not a cDC feature.

Gene/peak set enrichment analysis

Moderated $\log_2$FCs calculated by DESeq2 were used as input for ranking by GAGE (v.2.24.0)(Luo et al., 2009). Lists of transcriptional or epigenetic signatures were used as gene/peak sets to calculate P values. Only signatures that showed a q-value < 10^{-10} were considered significant and plotted as a bar plot.

Motif analysis

De novo analysis was performed using HOMER (v.4.9.1; Heinz et al., 2010) using the findMotifsGenome function, with the parameters "-size given -len 6,8,10,12 -mset vertebrates -mask" and using the entire ATAC-seq atlas as background.

Quantification and statistical analysis

All numerical results are presented as median with individual values shown in graphs. Normal distribution of data was not assumed, and statistical significance of differences between experimental groups was determined by nonparametric Mann–Whitney test. Differences were considered significant for P values <0.05 (*), <0.01 (**), and <0.001 (***). The number of animals per group (n) is indicated in the respective figure legends. All statistical calculations were performed using Prism (GraphPad) except for expression and chromatin analysis, for which R (v.3.3.2) was used.

Data and software availability

ATAC-seq and RNA-seq datasets have been deposited in the Gene Expression Omnibus repository under accession no. GSE106408 (GSE106405 for ATAC-seq and GSE106406 for RNA-seq).

Online supplemental material

Fig. S1 presents additional characterization of Etv6-deficient DC populations in vivo. Fig. S2 describes transcriptional (RNA-seq) and open chromatin (ATAC-seq) signatures of primary splenic DC subsets. Fig. S3 presents additional characterization of DC functions following the deletion of Etv6. Tables S1, S2, S3,

and S4 present gene expression as determined by RNA-seq in control and Etv6-deficient splenic DC subsets, including cDC1 (Table S1), Esam^{hi} cDC2 (Table S2), Esam^{lo} cDC2 (Table S3), and pDC (Table S4). Table S5 lists gene expression signatures of splenic DC subsets. Tables S6, S7, and S8 present open chromatin peaks as determined by ATAC-seq in control and Etv6-deficient splenic DC subsets, including cDC1 (Table S6), pDC (Table S7), and cDC2 (Table S8). Table S9 lists open chromatin signatures of splenic DC subsets.

Acknowledgments

We thank H. Salmon, M. Merad, M. Vaeth and S. Feske for reagents and advice.

This work was supported by National Institutes of Health grants AI072571, AG049074 and AI115382 (B. Reizis), AI100853 (C.M. Lau and O. A. Perez), AI124661 (M.E. Kirkling), and AI134040 (G.S. Yap). I. Tiniakou is a recipient of the Dr. Bernard Levine Postdoctoral Fellowship in Immunology.

The authors declare no competing financial interests.

Author contributions: C.M. Lau, I. Tiniakou, O. A. Perez, and M.E. Kirkling performed and interpreted experiments. G.S. Yap and H. Hock provided essential reagents. B. Reizis supervised the project. C.M. Lau, I. Tiniakou, and B. Reizis wrote the original manuscript. All authors reviewed and edited the manuscript.

Submitted: 20 December 2017
Revised: 19 June 2018
Accepted: 18 July 2018

References

Aliberti, J., O. Schulz, D.J. Pennington, H. Tsujimura, C. Reis e Sousa, K. Ozato, and A. Sher. 2003. Essential role for ICSBP in the in vivo development of murine CD8alpha + dendritic cells. *Blood.* 101:305–310. https://doi.org/10.1182/blood-2002-04-1088

Boisclair Lachance, J.F., N. Peláez, J.J. Cassidy, J.L. Webber, I. Rebay, and R.W. Carthew. 2014. A comparative study of Pointed and Yan expression reveals new complexity to the transcriptional networks downstream of receptor tyrosine kinase signaling. *Dev. Biol.* 385:263–278. https://doi.org/10.1016/j.ydbio.2013.11.002

Bolger, A.M., M. Lohse, and B. Usadel. 2014. Trimmomatic: a flexible trimmer for Illumina sequence data. *Bioinformatics.* 30:2114–2120. https://doi.org/10.1093/bioinformatics/btu170

Buenrostro, J.D., B. Wu, H.Y. Chang, and W.J. Greenleaf. 2015. ATAC-seq: A Method for Assaying Chromatin Accessibility Genome-Wide. *Curr. Protoc. Mol. Biol.* 109:21–29.

Caton, M.L., M.R. Smith-Raska, and B. Reizis. 2007. Notch-RBP-J signaling controls the homeostasis of CD8- dendritic cells in the spleen. *J. Exp. Med.* 204:1653–1664. https://doi.org/10.1084/jem.20062648

de Luca, C., T.J. Kowalski, Y. Zhang, J.K. Elmquist, C. Lee, M.W. Kilimann, T. Ludwig, S.M. Liu, and S.C. Chua Jr. 2005. Complete rescue of obesity, diabetes, and infertility in db/db mice by neuron-specific LEPR-B transgenes. *J. Clin. Invest.* 115:3484–3493. https://doi.org/10.1172/JCI24059

Falo, L.D. Jr., M. Kovacsovics-Bankowski, K. Thompson, and K.L. Rock. 1995. Targeting antigen into the phagocytic pathway in vivo induces protective tumour immunity. *Nat. Med.* 1:649–653. https://doi.org/10.1038/nm0795-649

Fuertes, M.B., A.K. Kacha, J. Kline, S.R. Woo, D.M. Kranz, K.M. Murphy, and T.F. Gajewski. 2011. Host type I IFN signals are required for antitumor CD8+ T cell responses through CD8alpha+ dendritic cells. *J. Exp. Med.* 208:2005–2016. https://doi.org/10.1084/jem.20101159

Graham, T.G., S.M. Tabei, A.R. Dinner, and I. Rebay. 2010. Modeling bistable cell-fate choices in the Drosophila eye: qualitative and quantitative perspectives. *Development.* 137:2265–2278. https://doi.org/10.1242/dev.044826

Grajales-Reyes, G.E., A. Iwata, J. Albring, X. Wu, R. Tussiwand, W. Kc, N.M. Kretzer, C.G. Briseño, V. Durai, P. Bagadia, et al. 2015. Batf3 maintains autoactivation of Irf8 for commitment of a CD8α(+) conventional DC clonogenic progenitor. *Nat. Immunol.* 16:708–717. https://doi.org/10.1038/ni.3197

Guilliams, M., F. Ginhoux, C. Jakubzick, S.H. Naik, N. Onai, B.U. Schraml, E. Segura, R. Tussiwand, and S. Yona. 2014. Dendritic cells, monocytes and macrophages: a unified nomenclature based on ontogeny. *Nat. Rev. Immunol.* 14:571–578. https://doi.org/10.1038/nri3712

Hacker, C., R.D. Kirsch, X.S. Ju, T. Hieronymus, T.C. Gust, C. Kuhl, T. Jorgas, S.M. Kurz, S. Rose-John, Y. Yokota, and M. Zenke. 2003. Transcriptional profiling identifies Id2 function in dendritic cell development. *Nat. Immunol.* 4:380–386. https://doi.org/10.1038/ni903

Hahne, F., and R. Ivanek. 2016. Visualizing Genomic Data Using Gviz and Bioconductor. *Methods Mol. Biol.* 1418:335–351. https://doi.org/10.1007/978-1-4939-3578-9_16

Heinz, S., C. Benner, N. Spann, E. Bertolino, Y.C. Lin, P. Laslo, J.X. Cheng, C. Murre, H. Singh, and C.K. Glass. 2010. Simple combinations of lineage-determining transcription factors prime cis-regulatory elements required for macrophage and B cell identities. *Mol. Cell.* 38:576–589. https://doi.org/10.1016/j.molcel.2010.05.004

Heng, T.S., and M.W. Painter. Immunological Genome Project Consortium. 2008. The Immunological Genome Project: networks of gene expression in immune cells. *Nat. Immunol.* 9:1091–1094. https://doi.org/10.1038/ni1008-1091

Hildner, K., B.T. Edelson, W.E. Purtha, M. Diamond, H. Matsushita, M. Kohyama, B. Calderon, B.U. Schraml, E.R. Unanue, M.S. Diamond, et al. 2008. Batf3 deficiency reveals a critical role for CD8alpha+ dendritic cells in cytotoxic T cell immunity. *Science.* 322:1097–1100. https://doi.org/10.1126/science.1164206

Hock, H., and A. Shimamura. 2017. ETV6 in hematopoiesis and leukemia predisposition. *Semin. Hematol.* 54:98–104. https://doi.org/10.1053/j.seminhematol.2017.04.005

Hock, H., E. Meade, S. Medeiros, J.W. Schindler, P.J. Valk, Y. Fujiwara, and S.H. Orkin. 2004. Tel/Etv6 is an essential and selective regulator of adult hematopoietic stem cell survival. *Genes Dev.* 18:2336–2341. https://doi.org/10.1101/gad.1239604

Hollenhorst, P.C., L.P. McIntosh, and B.J. Graves. 2011. Genomic and biochemical insights into the specificity of ETS transcription factors. *Annu. Rev. Biochem.* 80:437–471. https://doi.org/10.1146/annurev.biochem.79.081507.103945

Humblin, E., M. Thibaudin, F. Chalmin, V. Derangère, E. Limagne, C. Richard, R.A. Flavell, S. Chevrier, S. Ladoire, H. Berger, et al. 2017. IRF8-dependent molecular complexes control the Th9 transcriptional program. *Nat. Commun.* 8:2085. https://doi.org/10.1038/s41467-017-01070-w

Kc, W., A.T. Satpathy, A.S. Rapaport, C.G. Briseño, X. Wu, J.C. Albring, E.V. Russler-Germain, N.M. Kretzer, V. Durai, S.P. Persaud, et al. 2014. L-Myc expression by dendritic cells is required for optimal T-cell priming. *Nature.* 507:243–247. https://doi.org/10.1038/nature12967

Kent, W.J., A.S. Zweig, G. Barber, A.S. Hinrichs, and D. Karolchik. 2010. BigWig and BigBed: enabling browsing of large distributed datasets. *Bioinformatics.* 26:2204–2207. https://doi.org/10.1093/bioinformatics/btq351

Kirkling, M.E., U. Cytlak, C.M. Lau, K.L. Lewis, A. Resteu, A. Khodadadi-Jamayran, C.W. Siebel, H. Salmon, M. Merad, A. Tsirigos, et al. 2018. Notch signaling facilitates in vitro generation of cross-presenting classical dendritic cells. *Cell Reports.* 23:3658–3672.e6. https://doi.org/10.1016/j.celrep.2018.05.068

Kuwata, T., C. Gongora, Y. Kanno, K. Sakaguchi, T. Tamura, T. Kanno, V. Basrur, R. Martinez, E. Appella, T. Golub, and K. Ozato. 2002. Gamma interferon triggers interaction between ICSBP (IRF-8) and TEL, recruiting the histone deacetylase HDAC3 to the interferon-responsive element. *Mol. Cell. Biol.* 22:7439–7448. https://doi.org/10.1128/MCB.22.21.7439-7448.2002

Langmead, B., and S.L. Salzberg. 2012. Fast gapped-read alignment with Bowtie 2. *Nat. Methods.* 9:357–359. https://doi.org/10.1038/nmeth.1923

Lawrence, M., W. Huber, H. Pagès, P. Aboyoun, M. Carlson, R. Gentleman, M.T. Morgan, and V.J. Carey. 2013. Software for computing and annotating genomic ranges. *PLOS Comput. Biol.* 9:e1003118. https://doi.org/10.1371/journal.pcbi.1003118

Lewis, K.L., M.L. Caton, M. Bogunovic, M. Greter, L.T. Grajkowska, D. Ng, A. Klinakis, I.F. Charo, S. Jung, J.L. Gommerman, et al. 2011. Notch2 recep-

tor signaling controls functional differentiation of dendritic cells in the spleen and intestine. *Immunity.* 35:780–791. https://doi.org/10.1016/j.immuni.2011.08.013

Li, H., B. Handsaker, A. Wysoker, T. Fennell, J. Ruan, N. Homer, G. Marth, G. Abecasis, R. Durbin, and G.P.D. Proc. 1000 Genome Project Data Processing Subgroup. 2009. The Sequence Alignment/Map format and SAMtools. *Bioinformatics.* 25:2078–2079. https://doi.org/10.1093/bioinformatics/btp352

Li, Q.H., J.B. Brown, H.Y. Huang, and P.J. Bickel. 2011. Measuring Reproducibility of High-Throughput Experiments. *Ann. Appl. Stat.* 5:1752–1779. https://doi.org/10.1214/11-AOAS466

Liu, M., W. Gao, J.C. van Velkinburgh, Y. Wu, B. Ni, and Y. Tian. 2016. Role of Ets Proteins in Development, Differentiation, and Function of T-Cell Subsets. *Med. Res. Rev.* 36:193–220. https://doi.org/10.1002/med.21361

Love, M.I., W. Huber, and S. Anders. 2014. Moderated estimation of fold change and dispersion for RNA-seq data with DESeq2. *Genome Biol.* 15:550. https://doi.org/10.1186/s13059-014-0550-8

Luo, W., M.S. Friedman, K. Shedden, K.D. Hankenson, and P.J. Woolf. 2009. GAGE: generally applicable gene set enrichment for pathway analysis. *BMC Bioinformatics.* 10:161. https://doi.org/10.1186/1471-2105-10-161

Mabbott, N.A., J.K. Baillie, H. Brown, T.C. Freeman, and D.A. Hume. 2013. An expression atlas of human primary cells: inference of gene function from coexpression networks. *BMC Genomics.* 14:632. https://doi.org/10.1186/1471-2164-14-632

Mach, N., S. Gillessen, S.B. Wilson, C. Sheehan, M. Mihm, and G. Dranoff. 2000. Differences in dendritic cells stimulated in vivo by tumors engineered to secrete granulocyte-macrophage colony-stimulating factor or Flt3-ligand. *Cancer Res.* 60:3239–3246.

Mayordomo, J.I.T., T. Zorina, W.J. Storkus, L. Zitvogel, C. Celluzzi, L.D. Falo, C.J. Melief, S.T. Ildstad, W.M. Kast, A.B. Deleo, et al. 1995. Bone marrow-derived dendritic cells pulsed with synthetic tumour peptides elicit protective and therapeutic antitumour immunity. *Nat. Med.* 1:1297–1302. https://doi.org/10.1038/nm1295-1297

Merad, M., P. Sathe, J. Helft, J. Miller, and A. Mortha. 2013. The dendritic cell lineage: ontogeny and function of dendritic cells and their subsets in the steady state and the inflamed setting. *Annu. Rev. Immunol.* 31:563–604. https://doi.org/10.1146/annurev-immunol-020711-074950

Mildner, A., and S. Jung. 2014. Development and function of dendritic cell subsets. *Immunity.* 40:642–656. https://doi.org/10.1016/j.immuni.2014.04.016

Miller, J.C., B.D. Brown, T. Shay, E.L. Gautier, V. Jojic, A. Cohain, G. Pandey, M. Leboeuf, K.G. Elpek, J. Helft, et al. Immunological Genome Consortium. 2012. Deciphering the transcriptional network of the dendritic cell lineage. *Nat. Immunol.* 13:888–899. https://doi.org/10.1038/ni.2370

Naik, S.H., A.I. Proietto, N.S. Wilson, A. Dakic, P. Schnorrer, M. Fuchsberger, M.H. Lahoud, M. O'Keeffe, Q.X. Shao, W.F. Chen, et al. 2005. Cutting edge: generation of splenic CD8+ and CD8- dendritic cell equivalents in Fms-like tyrosine kinase 3 ligand bone marrow cultures. *J. Immunol.* 174:6592–6597. https://doi.org/10.4049/jimmunol.174.11.6592

Quinlan, A.R., and I.M. Hall. 2010. BEDTools: a flexible suite of utilities for comparing genomic features. *Bioinformatics.* 26:841–842. https://doi.org/10.1093/bioinformatics/btq033

Reis e Sousa, C., S. Hieny, T. Scharton-Kersten, D. Jankovic, H. Charest, R.N. Germain, and A. Sher. 1997. In vivo microbial stimulation induces rapid CD40 ligand-independent production of interleukin 12 by dendritic cells and their redistribution to T cell areas. *J. Exp. Med.* 186:1819–1829. https://doi.org/10.1084/jem.186.11.1819

Roberts, E.W., M.L. Broz, M. Binnewies, M.B. Headley, A.E. Nelson, D.M. Wolf, T. Kaisho, D. Bogunovic, N. Bhardwaj, and M.F. Krummel. 2016. Critical Role for CD103(+)/CD141(+) Dendritic Cells Bearing CCR7 for Tumor Antigen Trafficking and Priming of T Cell Immunity in Melanoma. *Cancer Cell.* 30:324–336. https://doi.org/10.1016/j.ccell.2016.06.003

Salmon, H., J. Idoyaga, A. Rahman, M. Leboeuf, R. Remark, S. Jordan, M. Casanova-Acebes, M. Khudoynazarova, J. Agudo, N. Tung, et al. 2016. Expansion and Activation of CD103(+) Dendritic Cell Progenitors at the Tumor Site Enhances Tumor Responses to Therapeutic PD-L1 and BRAF Inhibition. *Immunity.* 44:924–938. https://doi.org/10.1016/j.immuni.2016.03.012

Samie, M., and P. Cresswell. 2015. The transcription factor TFEB acts as a molecular switch that regulates exogenous antigen-presentation pathways. *Nat. Immunol.* 16:729–736. https://doi.org/10.1038/ni.3196

Sánchez-Paulete, A.R., F.J. Cueto, M. Martínez-López, S. Labiano, A. Morales-Kastresana, M.E. Rodríguez-Ruiz, M. Jure-Kunkel, A. Azpilikueta, M.A. Aznar, J.I. Quetglas, et al. 2016. Cancer Immunotherapy with Immunomodulatory Anti-CD137 and Anti-PD-1 Monoclonal Antibodies Requires BATF3-Dependent Dendritic Cells. *Cancer Discov.* 6:71–79. https://doi.org/10.1158/2159-8290.CD-15-0510

Satpathy, A.T., C.G. Briseño, J.S. Lee, D. Ng, N.A. Manieri, W. Kc, X. Wu, S.R. Thomas, W.L. Lee, M. Turkoz, et al. 2013. Notch2-dependent classical dendritic cells orchestrate intestinal immunity to attaching-and-effacing bacterial pathogens. *Nat. Immunol.* 14:937–948. https://doi.org/10.1038/ni.2679

Schraml, B.U., and C. Reis e Sousa. 2015. Defining dendritic cells. *Curr. Opin. Immunol.* 32:13–20. https://doi.org/10.1016/j.coi.2014.11.001

Sichien, D., C.L. Scott, L. Martens, M. Vanderkerken, S. Van Gassen, M. Plantinga, T. Joeris, S. De Prijck, L. Vanhoutte, M. Vanheerswynghels, et al. 2016. IRF8 Transcription Factor Controls Survival and Function of Terminally Differentiated Conventional and Plasmacytoid Dendritic Cells, Respectively. *Immunity.* 45:626–640. https://doi.org/10.1016/j.immuni.2016.08.013

Speir, M.L., A.S. Zweig, K.R. Rosenbloom, B.J. Raney, B. Paten, P. Nejad, B.T. Lee, K. Learned, D. Karolchik, A.S. Hinrichs, et al. 2016. The UCSC Genome Browser database: 2016 update. *Nucleic Acids Res.* 44(D1):D717–D725. https://doi.org/10.1093/nar/gkv1275

Spranger, S., D. Dai, B. Horton, and T.F. Gajewski. 2017. Tumor-Residing Batf3 Dendritic Cells Are Required for Effector T Cell Trafficking and Adoptive T Cell Therapy. *Cancer Cell.* 31:711–723.e714.

Steinman, R.M. 2012. Decisions about dendritic cells: past, present, and future. *Annu. Rev. Immunol.* 30:1–22. https://doi.org/10.1146/annurev-immunol-100311-102839

Yap, G.S., T. Scharton-Kersten, D.J. Ferguson, D. Howe, Y. Suzuki, and A. Sher. 1998. Partially protective vaccination permits the development of latency in a normally virulent strain of Toxoplasma gondii. *Infect. Immun.* 66:4382–4388.

Yarovinsky, F., D. Zhang, J.F. Andersen, G.L. Bannenberg, C.N. Serhan, M.S. Hayden, S. Hieny, F.S. Sutterwala, R.A. Flavell, S. Ghosh, and A. Sher. 2005. TLR11 activation of dendritic cells by a protozoan profilin-like protein. *Science.* 308:1626–1629. https://doi.org/10.1126/science.1109893

Zhang, Y., T. Liu, C.A. Meyer, J. Eeckhoute, D.S. Johnson, B.E. Bernstein, C. Nusbaum, R.M. Myers, M. Brown, W. Li, and X.S. Liu. 2008. Model-based analysis of ChIP-Seq (MACS). *Genome Biol.* 9:R137. https://doi.org/10.1186/gb-2008-9-9-r137

Zhu, L.J., C. Gazin, N.D. Lawson, H. Pagès, S.M. Lin, D.S. Lapointe, and M.R. Green. 2010. ChIPpeakAnno: a Bioconductor package to annotate ChIP-seq and ChIP-chip data. *BMC Bioinformatics.* 11:237. https://doi.org/10.1186/1471-2105-11-237